



Proceeding Paper

Impact of Aerosol Optical Properties, Precipitable Water, and Solar Geometry on Sky Radiances Using Radiative Transfer Modeling [†]

Christos-Panagiotis Giannaklis ^{1,*}, Stavros-Andreas Logothetis ¹, Vasileios Salamalikis ², Panayiotis Tzoumanikas ¹ and Andreas Kazantzidis ¹

¹ Laboratory of Atmospheric Physics, Department of Physics, University of Patras, GR 26500 Patras, Greece; logothetis_s@upnet.gr (S.-A.L.); tzumanik@ceid.upatras.gr (P.T.); akaza@upatras.gr (A.K.)

² NILU—Norwegian Institute for Air Research, 2027 Kjeller, Norway; vsal@nilu.no

* Correspondence: xristos_gia@hotmail.gr

[†] Presented at the 16th International Conference on Meteorology, Climatology and Atmospheric Physics—COMECAP 2023, Athens, Greece, 25–29 September 2023.

Abstract: Radiative transfer modeling is used to investigate the effect of aerosol optical properties and water vapor on cloud-free sky radiances at various atmospheric conditions. Simulations are generated by changing the most critical aerosol optical properties, namely aerosol optical depth, Ångström exponent, the single-scattering albedo, the precipitable water, and the solar zenith angle (SZA) in three different spectral ranges: ultraviolet A, visible, and near-infrared.

Keywords: aerosols; aerosol optical properties; water vapor; sky radiance; radiative transfer model

1. Introduction

The distribution of diffuse radiance over the sky hemisphere is frequently required in many fields and applications, like predicting the solar irradiance on sloped planes or a tilted solar collector [1], or to quantify the spectral angular effects on photovoltaic (PV) devices' performance [2,3]. Other solar applications include the prediction of irradiance incident on concentrating collectors [4], the calculation of the geometrical correction factor for a tilted sensor [5], and the evaluation of solar UV exposure of living organisms [6].

Sky radiance or luminance, in the absence of clouds, mainly depends on aerosols' optical properties. Aerosols influence the Earth's radiative budget by attenuating (scattering and absorbing) the incoming solar radiation (direct effect) and by acting as cloud condensation nuclei and changing the microphysical properties of clouds and their lifetime (indirect effect) [7]. Understanding the contribution of aerosols to radiative processes is often characterized by uncertainties due to the incomplete knowledge of aerosol microphysical and optical properties. In addition to that, the high spatiotemporal variability of both natural (e.g., volcanic eruption, desert dust, and sea-spray) and anthropogenic aerosols (e.g., biomass burning and engine fuel combustion) makes the problem particularly challenging. The intensity of scattered radiation and its angular distribution depends on the nature of the scatterer and its size in relation to the wavelength of the interacting radiation. The aerosol optical depth (AOD), the volume size distribution, the single-scattering albedo (SSA), the phase function and other aerosol optical properties (AOPs) were retrieved using an inversion algorithm based on measured or estimated sky radiances [8,9]. Different instruments exist to measure the sky radiance experimentally, such as sky scanners [10,11], radiometers [12], spectroradiometers [13,14] and, recently, all-sky imagers (ASIs) [14,15].

However, the limited number of stations around the globe that provide quality-assured solar data and the cost of the equipment lead to limited special coverage of sky radiance data. This has resulted in the development of sky radiance models that can be applied



Citation: Giannaklis, C.-P.; Logothetis, S.-A.; Salamalikis, V.; Tzoumanikas, P.; Kazantzidis, A. Impact of Aerosol Optical Properties, Precipitable Water, and Solar Geometry on Sky Radiances Using Radiative Transfer Modeling. *Environ. Sci. Proc.* **2023**, *26*, 106. <https://doi.org/10.3390/environsciproc2023026106>

Academic Editors: Konstantinos Moustiris and Panagiotis Nastos

Published: 28 August 2023



Copyright: © 2023 by the authors. Licensee MDPI, Basel, Switzerland. This article is an open access article distributed under the terms and conditions of the Creative Commons Attribution (CC BY) license (<https://creativecommons.org/licenses/by/4.0/>).

universally and provide accurate results under any atmospheric condition. Many empirical and semi-empirical approaches have been proposed for the determination of sky diffuse radiation, accompanied by certain limitations [16–19].

Radiative transfer modeling constitutes a valuable tool to accurately estimate the sky radiance/luminance [20–24]. These models take into account the optical depth of the atmosphere, the multiple extinction and scattering events at the atmosphere. A plane-parallel atmosphere is considered when solving the radiative transfer equation. In the present study, a sensitivity analysis of the clear-sky radiances is performed at various atmospheric conditions using the radiative transfer model libRadtran [25,26].

2. Radiative Transfer Simulations

LibRadtran provides a library for radiative transfer modeling and includes several functions for the calculation of solar and thermal radiation in the Earth's atmosphere. At the core of libRadtran lies the UVSPEC radiative transfer code. A radiative transfer model (RTM) calculates how extraterrestrial solar radiation is altered by its path through the atmosphere and the interactions with its constituents (namely, gases, aerosols, clouds). RTMs consider a plane-parallel atmosphere, i.e., a one-dimensional atmosphere bounded at the top and bottom by horizontal plane surfaces. Other assumptions made in the models worth mentioning include the fact that the medium (e.g., atmospheric layer) does not change with time as the photon passes through it, that the frequency of the photon does not change as it interacts with the matter, and that the photons move in straight lines.

To generate the sky's spectral radiance, version 2.0.1 of the libRadtran software package and the UVSPEC radiative transfer model are adopted. Different input values of AOD, the Ångström exponent (AE), single-scattering albedo (SSA), precipitable water (PW) and solar zenith angle (SZA) are selected to examine the effect of aerosol conditions to the sky luminance. We used DISORT (discrete-ordinate-method radiative transfer) method for solving the radiative transfer equation that assumes that the atmosphere consists of a number of adjacent homogenous layers.

3. Results

The simulated diffuse clear sky radiances are visually demonstrated as contour plots of the relative difference (%) of the radiances from a reference scenario at three solar zenith angles (10°, 40° and 70°) in three different spectral regions—ultraviolet A (UV-A, 320–400 nm), visible (VIS, 400–750 nm), and near-infrared (NIR, 750–2500 nm)—for the hemisphere above the horizon. Not all cases are presented in the current study. The ones with the most significant effect are selected.

Figure 1 shows the effect of AOD on the distribution of the diffuse sky radiance under cloud-free conditions at the visible spectral range. To explicitly quantify how the AOD affects the radiance simulations, the relative differences of the sky radiances were simulated by assuming no-aerosol and high-aerosol conditions in the atmosphere and calculated using Formula (1), as follows:

$$\text{Relative difference} = \frac{I_{\text{high-aerosols}} - I_{\text{no-aerosols}}}{I_{\text{no-aerosols}}} \quad (1)$$

It is clear that the presence of high aerosol load in the atmosphere results in extremely more scattered lights distributed in the sky with maximum values in the area near the Sun. As the aerosol load increases, the Mie scattering dominates over Rayleigh and the size of the solar disk increases, resulting in the above differences. For high SZA angles, the path of the incident light increases, as well as the interactions between the light beams and the aerosols, leading to more scattered radiation distributed in the sky. The above can be confirmed from the results in Figure 1.

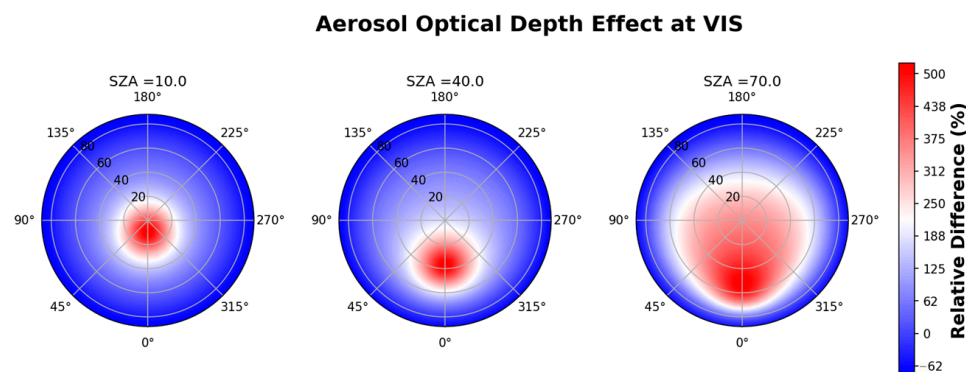


Figure 1. The effect of AOD on diffuse sky radiances in the visible spectral range. The color bar indicates the relative difference of radiance between high-aerosol and no-aerosol conditions in the atmosphere for SZA = 10° (left plot), SZA = 40° (middle plot), and SZA = 70° (right plot). The polar diagrams account for all the azimuth and solar angles for a given viewing angle of 0°.

In Figure 2, the effect of AE on the distribution of sky radiance is presented. The AE corresponds to the foremost aerosol size. The relative differences are calculated as for the AOD by comparing the cases with fine (AE = 1.9) and coarse (AE = 0.01) aerosol sizes. It is apparent that the coarse aerosols revealed a positive relative difference at scattering angles close to the circumsolar region due to Mie theory. At the edge of the polar plots, the sky radiances were higher for the fine aerosols. The latter comes to an agreement with the aerosol phase function for Mie theory.

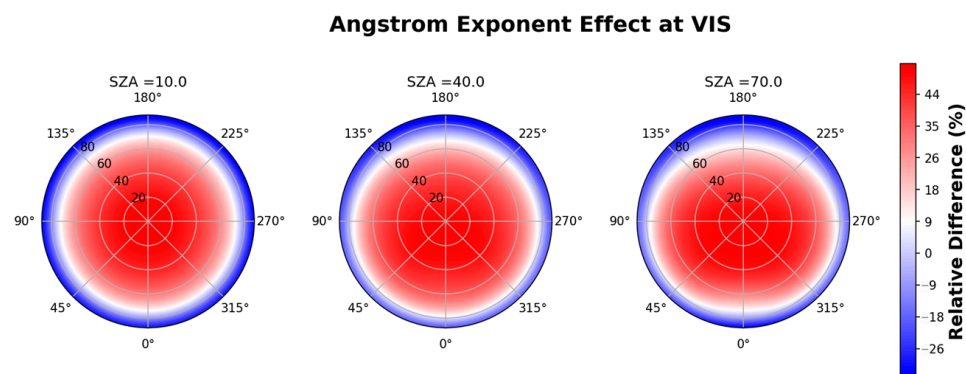


Figure 2. The effect of the AE on diffuse sky radiances in the visible spectral range. The color bar indicates the relative difference of radiance between fine aerosols (AE = 1.5) and coarse (AE = 0.0) aerosols for SZA = 10° (left plot), SZA = 40° (middle plot), and SZA = 70° (right plot). The polar diagrams account for all the azimuth and solar angles for a given viewing angle of 0°.

Figure 3 depicts the effect of SSA on the scattered radiation and its angular distribution. SSA is defined as the ratio of scattering to total extinction and corresponds to aerosol absorptivity. Higher SSA values signify that aerosols tend to scatter the solar radiation, while lower values reveal aerosols that are more absorbent. The relative differences are calculated as for the AOD and AE by comparing the cases with absorbing (SSA = 0.85) and non-absorbing (SSA = 0.99) aerosols. Based on Figure 3, for all scattering angles, the relative differences were positive, ranging from 26 to 56%. More specifically, at the edges of the polar plots, the relative differences were higher.



Figure 3. The effect of the SSA on diffuse sky radiances in the UV-A spectral range. The color bar indicates the relative difference of radiance between non-absorbing and absorbing SSA values for $SSA = 10^\circ$ (left plot), $SSA = 40^\circ$ (middle plot), and $SSA = 70^\circ$ (right plot) for an AOD of 0.5. The polar diagrams account for all the azimuth and solar angles for a given viewing angle of 0° .

Globally, water vapor absorbs in the visible and near-infrared solar spectrum more than any other atmospheric constituent. Under cloud-free conditions, water vapor absorbs the majority of the total solar absorption in the atmosphere. The predominance of the water vapor absorption occurs in near-infrared. With that considered, the effect of the PW in the diffuse radiance field in the NIF spectral range is shown in Figure 4. The absorption of PW leads to a decrease in the sky radiance of around 20–40%, with the highest differences occurring in the horizon.

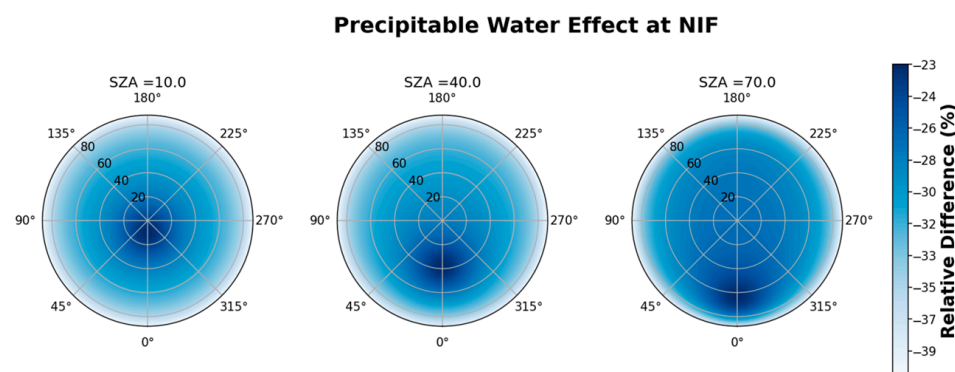


Figure 4. The effect of the PW on diffuse sky radiances in the NIF spectral range. The color bar indicates the relative difference of radiance between high-PW and no-PW values for $PW = 10^\circ$ (left plot), $PW = 40^\circ$ (middle plot), and $PW = 70^\circ$ (right plot). The polar diagrams account for all the azimuth and solar angles for a given viewing angle of 0° .

4. Conclusions

In this contribution, numerous radiative transfer simulations were performed to describe the spectral radiance of clear skies under different aerosol conditions. To cover a large range of cases, the clear sky radiance/luminance relative changes were calculated, varying AOD, AE, SSA, and PW for different solar geometries in three broadband wavelengths. The presented findings highlight the increase in diffuse sky radiance with high values of AOD and large SZAs, especially in the circumsolar region.

Author Contributions: Conceptualization, C.-P.G. and A.K.; methodology, C.-P.G.; software, C.-P.G. validation, C.-P.G., S.-A.L. and V.S.; formal analysis, C.-P.G.; investigation, C.-P.G.; data curation, C.-P.G. and P.T.; writing—original draft preparation, C.-P.G.; writing—review and editing, C.-P.G., S.-A.L. and V.S.; visualization, C.-P.G.; supervision, A.K.; funding acquisition, A.K. All authors have read and agreed to the published version of the manuscript.

Funding: This publication was funded by the Hellenic Foundation for Research and Innovation (H.F.R.I.) under the “2nd Call for H.F.R.I. Research Projects to support Faculty Members & Researchers” (Project Number: 4129).

Institutional Review Board Statement: Not applicable.

Informed Consent Statement: Not applicable.

Data Availability Statement: The data presented in this study are available on request from the corresponding author.

Acknowledgments: We acknowledge support of the project D3D to this study, supported by the Hellenic Foundation for Research and Innovation (H.F.R.I.) under the “2nd Call for H.F.R.I. Research Projects to support Faculty Members & Researchers” (Project Number: 4129).

Conflicts of Interest: The authors declare no conflict of interest.

References

- Li, D.H.; Lam, J.C. Predicting solar irradiance on inclined surfaces using sky radiance data. *Energy Convers. Manag.* **2004**, *45*, 1771–1783. [[CrossRef](#)]
- Plag, F.; Kröger, I.; Riechelmann, S.; Winter, S. Multidimensional model to correct PV device performance measurements taken under diffuse irradiation to reference conditions. *Sol. Energy* **2018**, *174*, 431–444. [[CrossRef](#)]
- Behrendt, T.; Kuehnert, J.; Hammer, A.; Lorenz, E.; Betcke, J.; Heinemann, D. Solar spectral irradiance derived from satellite data: A tool to improve thin film PV performance estimations? *Sol. Energy* **2013**, *98*, 100–110. [[CrossRef](#)]
- Suzuki, A.; Kobayashi, S. Yearly distributed insolation model and optimum design of a two dimensional compound parabolic concentrator. *Sol. Energy* **1995**, *54*, 327–331. [[CrossRef](#)]
- de Simón-Martín, M.; Díez-Mediavilla, M.; Alonso-Tristán, C. Shadow-band radiometer measurement of diffuse solar irradiance: Calculation of geometrical and total correction factors. *Sol. Energy* **2016**, *139*, 85–99. [[CrossRef](#)]
- Seckmeyer, G.; Schrenpf, M.; Wieczorek, A.; Riechelmann, S.; Graw, K.; Seckmeyer, S.; Zankl, M. A Novel Method to Calculate Solar UV Exposure Relevant to Vitamin D Production in Humans. *Photochem. Photobiol.* **2013**, *89*, 974–983. [[CrossRef](#)]
- Allen, S.K.; Barros, V.; Burton, I.; Campbell-Lendrum, D.; Cardona, O.-D.; Cutter, S.L.; Dube, O.P.; Ebi, K.L.; Field, C.B.; Handmer, J.W.; et al. Summary for Policymakers. In *Managing the Risks of Extreme Events and Disasters to Advance Climate Change Adaptations: Special Report of the Intergovernmental Panel on Climate Change*; Field, C., Barros, V., Stocker, T., Dahe, Q., Eds.; Cambridge University Press: Cambridge, UK, 2012; pp. 3–22. [[CrossRef](#)]
- Olmo, F.; Quirantes, A.; Lara, V.; Lyamani, H.; Alados-Arboledas, L. Aerosol optical properties assessed by an inversion method using the solar principal plane for non-spherical particles. *J. Quant. Spectrosc. Radiat. Transf.* **2007**, *109*, 1504–1516. [[CrossRef](#)]
- Dubovik, O.; King, M.D. A flexible inversion algorithm for retrieval of aerosol optical properties from Sun and sky radiance measurements. *J. Geophys. Res. Atmos.* **2000**, *105*, 20673–20696. [[CrossRef](#)]
- Tohsing, K.; Klomkliang, W.; Masiri, I.; Janjai, S. An investigation of sky radiance from the measurement at a tropical site. *AIP Conf. Proc.* **2017**, *1810*, 080006. [[CrossRef](#)]
- Wuttke, S.; Seckmeyer, G. Spectral radiance and sky luminance in Antarctica: A case study. *Theor. Appl. Clim.* **2006**, *85*, 131–148. [[CrossRef](#)]
- Nakajima, T.; Campanelli, M.; Che, H.; Estellés, V.; Irie, H.; Kim, S.-W.; Kim, J.; Liu, D.; Nishizawa, T.; Pandithurai, G.; et al. An overview of and issues with sky radiometer technology and SKYNET. *Atmospheric Meas. Tech.* **2020**, *13*, 4195–4218. [[CrossRef](#)]
- Kider, J.T.; Knowlton, D.; Newlin, J.; Li, Y.K.; Greenberg, D.P. A framework for the experimental comparison of solar and skydome illumination. *ACM Trans. Graph.* **2014**, *33*, 1–12. [[CrossRef](#)]
- Ricchiuzzi, P.J.; Payton, A.; Gautier, C. The Effect of Surface Albedo Heterogeneity on Sky Radiance. In Proceedings of the Tenth ARM Science Team Meeting, San Antonio, TX, USA, 13–17 March 2000.
- Tohsing, K.; Schrenpf, M.; Riechelmann, S.; Seckmeyer, G. Validation of spectral sky radiance derived from all-sky camera images – A case study. *Atmos. Meas. Tech.* **2014**, *7*, 2137–2146. [[CrossRef](#)]
- Perez, R.; Seals, R.; Michalsky, J. All-weather model for sky luminance distribution—Preliminary configuration and validation. *Sol. Energy* **1993**, *50*, 235–245. [[CrossRef](#)]
- Mardaljevic, J. Sky model blends for predicting internal illuminance: A comparison founded on the BRE-IDMP dataset. *J. Build. Perform. Simul.* **2008**, *1*, 163–173. [[CrossRef](#)]
- Ferraro, V.; Mele, M.; Marinelli, V. Analysis of sky luminance experimental data and comparison with calculation methods. *Energy* **2012**, *37*, 287–298. [[CrossRef](#)]
- Igawa, N. Improving the All Sky Model for the luminance and radiance distributions of the sky. *Sol. Energy* **2014**, *105*, 354–372. [[CrossRef](#)]
- Liang, S.; Lewis, P. A parametric radiative transfer model for sky radiance distribution. *J. Quant. Spectrosc. Radiat. Transf.* **1996**, *55*, 181–189. [[CrossRef](#)]

21. Gueymard, C.A. Parameterized transmittance model for direct beam and circumsolar spectral irradiance. *Sol. Energy* **2001**, *71*, 325–346. [[CrossRef](#)]
22. Kocifaj, M. Angular distribution of scattered radiation under broken cloud arrays: An approximation of successive orders of scattering. *Sol. Energy* **2012**, *86*, 3575–3586. [[CrossRef](#)]
23. Kocifaj, M. Unified model of radiance patterns under arbitrary sky conditions. *Sol. Energy* **2015**, *115*, 40–51. [[CrossRef](#)]
24. Gueymard, C.A.; Kocifaj, M. Clear-sky spectral radiance modeling under variable aerosol conditions. *Renew. Sustain. Energy Rev.* **2022**, *168*. [[CrossRef](#)]
25. Mayer, B.; Kylling, A. Technical note: The libRadtran software package for radiative transfer calculations - description and examples of use. *Atmos. Chem. Phys.* **2005**, *5*, 1855–1877. [[CrossRef](#)]
26. Emde, C.; Buras-Schnell, R.; Kylling, A.; Mayer, B.; Gasteiger, J.; Hamann, U.; Kylling, J.; Richter, B.; Pause, C.; Dowling, T.; et al. The libRadtran software package for radiative transfer calculations (version 2.0.1). *Geosci. Model Dev.* **2016**, *9*, 1647–1672. [[CrossRef](#)]

Disclaimer/Publisher’s Note: The statements, opinions and data contained in all publications are solely those of the individual author(s) and contributor(s) and not of MDPI and/or the editor(s). MDPI and/or the editor(s) disclaim responsibility for any injury to people or property resulting from any ideas, methods, instructions or products referred to in the content.